Showcasing collaborative research from Professor Serena Corr's laboratory, School of Chemistry, University of Glasgow and Dr Edmund Cussen, Department of Pure and Applied Chemistry, University of Strathclyde, Glasgow, United Kingdom.

$Na_{1.5}La_{1.5}TeO_6$: Na$^+$ conduction in a novel Na-rich double perovskite

Bridging of contiguous Na ions in the novel $Na_{1.5}La_{1.5}TeO_6$ Na-rich double perovskite ionic conductor material is enabled by the presence of Na ions in both A- and B-sites, resulting in a lower energy barrier for Na-ion diffusion.

ROYAL SOCIETY
OF **CHEMISTRY**

rsc.li/chemcomm

Registered charity number: 207890

ChemComm

Check for updates

Na$_{1.5}$La$_{1.5}$TeO$_6$: Na$^+$ conduction in a novel Na-rich double perovskite†

Marco Amores, [ID] [ab] Peter J. Baker, [ID] [c] Edmund J. Cussen [ID] [b] and Serena A. Corr [ID] *[a]

Increasing demand for lithium batteries for automotive applications, coupled with the necessity to move to large-scale energy storage systems, is driving a push towards new technologies and has seen Na-ion batteries emerge as a leading alternative to Li-ion. Amongst these, all solid-state configurations represent a promising route to achieving higher energy densities and increased safety. Remaining challenges include the need for Na$^+$ solid electrolytes with the requisite ionic conductivities crucial for use in a solid-state cell. Here, we present the novel Na-rich double perovskite, Na$_{1.5}$La$_{1.5}$TeO$_6$. The transport properties, explored at the macroscopic and local level, reveal a low activation energy barrier for Na$^+$ diffusion and great promise for use as an electrolyte for all solid-state Na-batteries.

The lower cost and greater availability of sodium compared to lithium, together with its similar redox couple potential of *ca.* 0.3 V lower for Na/Na$^+$ compared to Li/Li$^+$, has led to enormous interest in the development of Na batteries by the energy storage community over the last decade.[1] The larger cation size and heavier mass of sodium had made it a suitable candidate for medium to large-scale stationary energy storage applications, where gravimetric energy density is not a priority. As with Li-ion batteries, organic liquid Na-electrolytes present concerns in terms of safety and the operating voltage window available. The use of solid-state electrolytes in Na batteries could increase the energy density and safety of the battery, enable longer cyclability and permit the use of versatile cell geometries.[2,3] Current Na$^+$ solid-state electrolytes display Na$^+$ conductivities at room temperature from 10^{-10} S cm^{-1}, in the case of the Na(B/Al)H$_4$ complex hydrides, to benchmark values close to the mS cm^{-1} for the recently reported Na-containing chalcogenides.[2–4] Other systems include the NASICON phosphate

materials, the classic β''-Al$_2$O$_3$ and the more recent layered P2-type Na$_2$M$_2$TeO$_6$ materials.[2,5] The electrolyte choice should fit the specific battery application, operating temperature and electrode in order to avoid malfunction. For example, β''-Al$_2$O$_3$ degrades with moisture content[6] and the room temperature superionic Na-containing sulfide materials suffer from poor electrochemical stability and reaction with Na metal electrodes.[7] Therefore, research on new Na$^+$ solid-state electrolyte systems that could meet requirements lacking in present systems is critical. Here, we present a new sodium-rich solid-state electrolyte Na$_{1.5}$La$_{1.5}$TeO$_6$, where the robust perovskite framework and redox stability of the Te^{6+} ions[8–12] could enable its use in combination with high voltage electrodes.

A$_2$BB'O$_6$ double perovskite structure allows for a wide range of potential compositions with multiple combinations of elements on the A, B and B' sites, where B and B' cation positions are ordered in the crystal structure.[13] The novel Na-rich Na$_{1.5}$La$_{1.5}$TeO$_6$ double perovskite presented here crystallises in the monoclinic P2$_1$/n space group, with 1 mol of Na$^+$ and 1 mol of Te^{6+} cations occupying the octahedral B and B' sites in a rock-salt type ordered fashion (Fig. 1). From the 2 mols of 8-fold coordinate A-sites, 1.5 mol is occupied by La^{3+} cations and 0.5 mols are occupied by additional Na$^+$, producing a ''Na-rich'' double perovskite with an expanded formula unit of Na$_{0.5}$La$_{1.5}$NaTeO$_6$. A similar alkali-metal rich double perovskite was reported by Rosseinsky and co-workers for the Li$_{1.5}$La$_{1.5}$WO$_6$ composition.[14] The discrepancy between the charges and sizes of the cations sitting in the A and BB' sites produces the distortion of the symmetry from the ideal cubic structure to a monoclinic symmetry through an a$^-$a$^-$b$^+$ tilting system, as expected for a tolerance factor of 0.83 calculated for the Na$_{1.5}$La$_{1.5}$TeO$_6$ composition. The synthesis of Na$_{1.5}$La$_{1.5}$TeO$_6$ was achieved though an energy-efficient microwave-assisted solid-state synthesis. Such routes have been developed by our group in recent years for Li$^+$ solid electrolytes,[15–18] where the presence of hydroxide and oxide precursors increase the reaction kinetics by coupling effectively to microwave irradiation.[19]

[a] *School of Chemistry, University of Glasgow, Glasgow G12 8QQ, UK.*
  E-mail: Serena.Corr@glasgow.ac.uk

[b] *Department of Pure and Applied Chemistry, The University of Strathclyde,*
  Thomas Graham Building, 295 Cathedral Street, Glasgow, G1 1XL, UK

[c] *ISIS Pulsed Neutron and Muon Source, STFC Rutherford Appleton Laboratory,*
  Harwell Science and Innovation Campus, Didcot, Oxfordshire OX11 0QX, UK

† Electronic supplementary information (ESI) available. See DOI: 10.1039/c8cc03367f
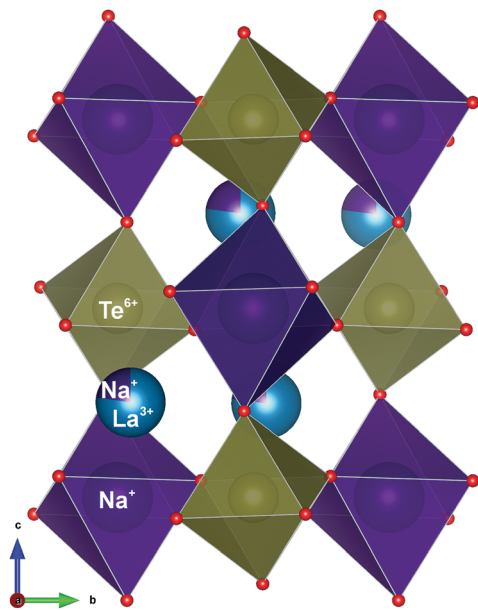
Fig. 1 Crystallographic representation of the $Na_{1.5}La_{1.5}TeO_6$ structure with monoclinic symmetry $P2_1/n$, where brown spheres represent octahedrally coordinated Te^{6+} ions, blue spheres represent 8-fold coordinated La^{3+} ions, purple spheres are the Na^+ ions and the oxygen anions are represented in red.
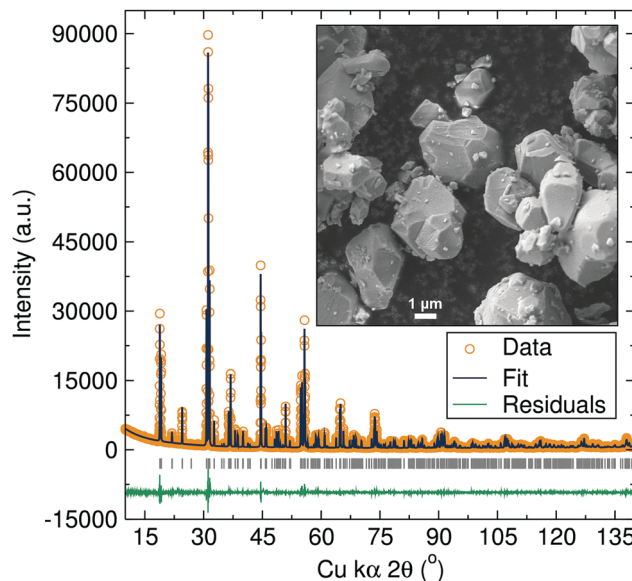

Fig. 2 Rietveld refinements of XRD data for the $Na_{1.5}La_{1.5}TeO_6$ double perovskite to the $P2_1/n$ monoclinic space group. Bragg peaks positions for the monoclinic $P2_1/n$ structure are indicated by vertical grey tick marks. Fit in excellent agreement to monoclinic space group $P2_1/n$, with cell parameters a = 5.69186(2) Å, b = 5.83933(2) Å, c = 8.13119(3) Å, β = 90.186(1)° and V = 270.253(1) Å³. R_{wp} = 0.0743, R_{exp} = 0.0530 and χ^2 = 7.051. Inset: SEM image of $Na_{1.5}La_{1.5}TeO_6$ double perovskite.

The structure of the $Na_{1.5}La_{1.5}TeO_6$ double perovskite with monoclinic $P2_1/n$ symmetry was established by Rietveld refinements of powder XRD data (Fig. 2). As expected, Na^+ and Te^{6+} cations occupy the rock salt ordered B and B′ sites and refinement of site occupancies (Table S1, ESI†) indicated the presence of ∼25% vacancies on the La^{3+} occupying the A-site, reminiscent of the related $Li_{1.5}La_{1.5}WO_6$ double perovskite.[14] Na^+ was refined into these vacant A-sites unoccupied by the La^{3+}, giving an A-site occupancy for this additional Na^+ of 0.239(2) which fills the available A-site vacancies. The calculated angle for the Na_B–O–Te was 152.1(4)°, resulting in a Glazer tilt of 13.9°, in good agreement with the related $Li_{1.5}La_{1.5}WO_6$ material (∼13.6°).[14] The precision in the atomic parameters of Na^+ and O^{2-} is necessarily lower than for the stronger X-ray scatters La^{3+} and Te^{6+}, but the high atomic displacement parameters of the Na^+ ions may be indicative of mobility. The stoichiometry from Rietveld refinement was found to be $Na_{1.48(1)}La_{1.534(4)}TeO_6$, which was further confirmed by EDX analyses, where an atomic ratio of $Na_{1.52(8)}La_{1.48(4)}Te_{1.00(4)}$ was found (Fig. S2, ESI†), in excellent agreement with XRD and the target stoichiometry. Raman analysis (Fig. S1, ESI†) also confirmed the presence of vibrational bands corresponding to the monoclinic $P2_1/n$ group and the absence of carbonate or hydroxide moieties that could arise from secondary phases, typically invisible to laboratory XRD. The material microstructure was studied by SEM (Fig. 2 inset). The $Na_{1.5}La_{1.5}TeO_6$ particles had sizes ranging from 1 to 5 μm, with irregular, faceted morphologies.

To investigate the ionic macro- and microtransport properties of the $Na_{1.5}La_{1.5}TeO_6$ materials, electrochemical impedance spectroscopy and muon spin relaxation measurements (μ⁺SR)

were carried out. Fig. 3a shows the Nyquist plots of the impedance measurements, where two main components are observed. A semicircle component is noted at high frequencies, due to the resistance of the material towards ionic diffusion, and a second component in form of a linear tail can be seen at low frequencies resulting from the sodium-blocking gold electrodes employed in these measurements, indicating the predominantly ionic character of the observed impedance.[20] These data were fitted using equivalent electrical circuit composed of a resistor in parallel with a constant phase element, in series with a Warburg resistance. This gave a value for the ionic conductivity of $Na_{1.5}La_{1.5}TeO_6$ at room temperature of 5.4×10^{-8} S cm⁻¹. This is on the order of that first reported for phosphate NASICON materials, which has since seen improvements up to 10^{-3} S cm⁻¹ through stoichiometric and structure-tailoring strategies.[21–25] These structure-tailoring strategies include element substitutions in the NASICON framework to increase the carrier concentrations or to increase the conduction channel size and hence the ionic conductivity of these materials.[26,27] In the case of the P2-type $Na_2M_2TeO_6$ tellurates oxides materials, the original work reported conductivities of 10^{-6} S cm⁻¹ which have been now optimized to reach the mS cm⁻¹ range.[5,12] It is reasonable to expect therefore that similar improvements are possible for the $Na_{1.5}La_{1.5}TeO_6$ double perovskite presented here through, for example, aliovalent doping or morphological control.

The activation energy required for macroscopic ionic conduction, calculated from an Arrhenius plot of EIS data, showed a promising value of 0.27(2) eV (Fig. 3c). This value is significantly lower compared to that obtained for the analogous
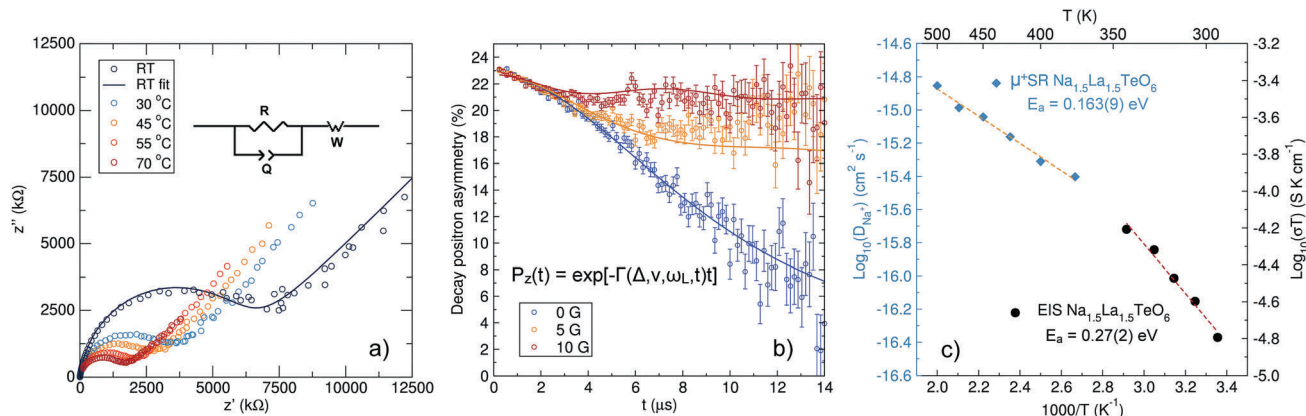
Fig. 3 (a) Nyquist plot of EIS data for $Na_{1.5}La_{1.5}TeO_6$ at different temperatures and a representative fit to the equivalent electrical circuit. (b) Room temperature μ^+SR data collected for $Na_{1.5}La_{1.5}TeO_6$ at zero field and applied longitudinal fields of 5 G and 10 G, fitted (solid lines) using the Keren function. (c) Arrhenius plots of the ionic conductivity and diffusion coefficient of $Na_{1.5}La_{1.5}TeO_6$ from μ^+SR and EIS.

$Li_{1.5}La_{1.5}WO_6$ double perovskite material of 0.50(5) eV.[14] This lower energetic requirement for ionic diffusion found for $Na_{1.5}La_{1.5}TeO_6$ could be related to the high relative density of the sintered material, nearly 96%, which results in a lower inter-grain energy requirement for Na^+ diffusion between sintered particles. The macroscopic activation energy found for this Na-rich double perovskite is similar to current benchmark systems with low activation energy values from EIS measurements,[2,3,28] for example Na_3PSe_4 which displays an activation energy of 0.21 eV.[29] Preliminary EIS analysis of a Na-metal electrode-sandwiched $Na_{1.5}La_{1.5}TeO_6$ cell at 80 °C revealed the lack of a Warburg element, confirming Na^+ as the conducting species (Fig. S3, ESI†). An increase in impedance over time is observed, which may point to a reaction with the sodium metal electrode at this temperature. Further examination of this, together with the use of similar protection approaches used for Li-metal anodes, could overcome these compatibility issues at high temperatures.[30,31]

The local Na^+ diffusion properties were also investigated by μ^+SR measurements performed on the EMU instrument at the ISIS Neutron and Muon source. The use of μ^+SR as a local probe to study Li^+ and Na^+ diffusion in battery materials has grown in recent years.[15,32–34] The natural abundance of the spin 1/2 ^{23}Na isotope is 100%, making Na^+ an ideal candidate to be studied by μ^+SR. The temporal evolution of the decay positron asymmetry for $Na_{1.5}La_{1.5}TeO_6$ at three different longitudinal magnetic fields is shown in Fig. 3b. At short times, the decay positron asymmetry followed a moderate decay, while at longer times the asymmetry decrease followed a slower trend, as expected for this Na-rich double perovskite with no para-magnetic ions in its structure and which also contains active nuclear spins (^{23}Na, ^{139}La and ^{125}Te) which can interact with the muon spin. To obtain the fluctuation rate of the muons due to sodium-ion diffusion (Fig. S4, ESI†), the muon decay asymmetry data were fitted using Keren's analytic generalization of the Abragam function (Fig. 3b).[35] The Na^+ diffusion coefficients from the muon fluctuation rate at different temperatures were then calculated applying eqn (1),[36] where N_i is the number

of accessible Na sites in the i-th path, $Z_{v,i}$ is the vacancy fraction of the destination sites, s_i the jump distance between Na^+ sites, and ν the calculated muon fluctuation rate at each temperature.

$$D_{Na^+} = \sum_{i=1}^{n} \frac{1}{N_i} Z_{v,i} s_i^2 \nu \qquad (1)$$

Since a detailed model of the Na^+ diffusion pathways for this novel Na-rich double perovskite is still not available, a simplified model based on the calculations reported by Rosseinsky and co-workers for the $Li_{1.5}La_{1.5}WO_6$ perovskite was employed.[14] The model is shown in Fig. S5 (ESI†) where Na^+ diffuses from the A sites to the two neighbouring B sites and from the B sites to the four neighbouring A sites, creating a 3D network for Na^+ diffusion. Additionally, a conservative 0.01 vacancy fraction in the Na^+ positions was introduced in both A and B sites to allow diffusion. From this preliminary model, and introducing the two different Na_A–Na_B distances of 3.33 and 3.46 Å, a Na^+ diffusion coefficient at room temperature of 4.2×10^{-12} cm^2 s^{-1} was obtained. This diffusion coefficient is similar to that reported for the $Na_x(Mn/Co)O_2$ layered cathode materials (10^{-11}–10^{-12} cm^2 s^{-1}), indicating excellent compatibility of these components in terms of Na^+ diffusion.[34,37,38] The microscopic diffusion of $Na_{1.5}La_{1.5}TeO_6$ is also in line with other Na^+ ionic conductors such as the $Na_xWO_2Cl_2$ tungsten bronze with a Na^+ diffusion coefficient of 10^{-13} cm^2 s^{-1},[39] and Na_3PS_4 with a value in the range of 10^{-12} cm^2 s^{-1}.[40] The μ^+SR measurements indicate that the activation energy required for local Na^+ diffusion is 0.163(9) eV. This low activation energy is similar to related oxide materials, such as the Ga-doped $Na_2Zn_2TeO_6$ with an activation energy of 0.12 eV as observed from NMR measurements,[12] or β'-alumina single crystals with activations energies in the 0.12–0.16 eV range.[41]

The higher activation energy values obtained from the macroscopic EIS measurements which probes long range Na^+ conduction through multiple intra-grain crystalline sites and grain boundaries, compared to microscopic μ^+SR measurements which are more sensitive to individual Na^+ hops within

the crystalline grain, could have its origin in the contribution to the resistance from grain boundaries to ionic conduction which is virtually invisible to μ^+SR. Lower conductivity values and higher energy barriers to diffusion could also result from the presence of La^{3+} ions in the A-sites, which could hinder long-range Na^+ conductivity. Nevertheless, the excellent microscopic Na^+ transport properties displayed by this novel $Na_{1.5}La_{1.5}TeO_6$ Na-rich double perovskite indicates that, upon further optimization, this material could be a promising candidate as a solid electrolyte for Na batteries.

In conclusion, we have demonstrated the synthesis of a novel Na-rich double perovskite, $Na_{1.5}La_{1.5}TeO_6$ through microwave methods, which crystallises with monoclinic $P2_1/n$ space group with Na^+ on both the A- and B-sites. The material displays a macroscopic ionic conductivity on the order of 10^{-8} S cm^{-1} at room temperature with a low activation energy of 0.27(2) eV. μ^+SR measurements reveal a microscopic diffusion coefficient for Na^+ at room temperature in the order of 10^{-12} cm^2 s^{-1} and a very low activation energy of 0.163(9) eV. These findings reveal the promising transport properties for this $Na_{1.5}La_{1.5}TeO_6$ material and further developments are forthcoming to optimize the macroscopic transport to its maximum microscopic potential.

Conflicts of interest

There are no conflicts to declare.

References

1 J.-Y. Hwang, S.-T. Myung and Y.-K. Sun, *Chem. Soc. Rev.*, 2017, **46**, 3529–3614.
2 J.-J. Kim, K. Yoon, I. Park and K. Kang, *Small Methods*, 2017, **1**, 1700219.
3 H. Che, S. Chen, Y. Xie, H. Wang, K. Amine, X.-Z. Liao and Z.-F. Ma, *Energy Environ. Sci.*, 2017, **10**, 1075–1101.
4 K. B. Hueso, M. Armand and T. Rojo, *Energy Environ. Sci.*, 2013, **6**, 734–749.
5 M. A. Evstigneeva, V. B. Nalbandyan, A. A. Petrenko, B. S. Medvedev and A. A. Kataev, *Chem. Mater.*, 2011, **23**, 1174–1181.
6 F. G. Will, *J. Electrochem. Soc.*, 1976, **123**, 834–836.
7 Z. Yu, S.-L. Shang, Y. Gao, D. Wang, X. Li, Z.-K. Liu and D. Wang, *Nano Energy*, 2018, **47**, 325–330.
8 A. Gupta, C. B. Mullins and J. B. Goodenough, *J. Power Sources*, 2013, **243**, 817–821.
9 M. Sathiya, K. Ramesha, G. Rousse, D. Foix, D. Gonbeau, K. Guruprakash, A. S. Prakash, M. L. Doublet and J.-M. Tarascon, *Chem. Commun.*, 2013, **49**, 11376–11378.
10 Z. Yang, Y. Jiang, L. Deng, T. Wang, S. Chen and Y. Huang, *J. Power Sources*, 2017, **360**, 319–323.
11 E. A. Zvereva, V. B. Nalbandyan, M. A. Evstigneeva, H.-J. Koo, M.-H. Whangbo, A. V. Ushakov, B. S. Medvedev, L. I. Medvedeva, N. A. Gridina, G. E. Yalovega, A. V. Churikov, A. N. Vasiliev and B. Büchner, *J. Solid State Chem.*, 2015, **225**, 89–96.
12 Y. Li, Z. Deng, J. Peng, E. Chen, Y. Yu, X. Li, J. Luo, Y. Huang, J. Zhu, C. Fang, Q. Li, J. Han and Y. Huang, *Chem. – Eur. J.*, 2018, **24**, 1057–1061.
13 S. Vasala and M. Karppinen, *Prog. Solid State Chem.*, 2015, **43**, 1–36.
14 A. B. Santibanez-Mendieta, C. Didier, K. K. Inglis, A. J. Corkett, M. J. Pitcher, M. Zanella, J. F. Shin, L. M. Daniels, A. Rakhmatullin, M. Li, M. S. Dyer, J. B. Claridge, F. Blanc and M. J. Rosseinsky, *Chem. Mater.*, 2016, **28**, 7833–7851.
15 M. Amores, T. E. Ashton, P. J. Baker, E. J. Cussen and S. A. Corr, *J. Mater. Chem. A*, 2016, **4**, 1729–1736.
16 M. Amores, S. A. Corr and E. J. Cussen, *J. Electrochem. Soc.*, 2017, **164**, A6395–A6400.
17 H. El-Shinawi, E. J. Cussen and S. A. Corr, *Dalton Trans.*, 2017, **46**, 9415–9419.
18 H. El-Shinawi, G. W. Paterson, D. A. MacLaren, E. J. Cussen and S. A. Corr, *J. Mater. Chem. A*, 2017, **5**, 319–329.
19 H. J. Kitchen, S. R. Vallance, J. L. Kennedy, N. Tapia-Ruiz, L. Carassiti, A. Harrison, A. G. Whittaker, T. D. Drysdale, S. W. Kingman and D. H. Gregory, *Chem. Rev.*, 2014, **114**, 1170–1206.
20 J. T. S. Irvine, D. C. Sinclair and A. R. West, *Adv. Mater.*, 1990, **2**, 132–138.
21 F. E. Mouahid, M. Bettach, M. Zahir, P. Maldonado-Manso, S. Bruque, E. R. Losilla and M. A. G. Aranda, *J. Mater. Chem.*, 2000, **10**, 2748–2757.
22 N. Anantharamulu, K. Koteswara Rao, G. Rambabu, B. Vijaya Kumar, V. Radha and M. Vithal, *J. Mater. Sci.*, 2011, **46**, 2821–2837.
23 H. Park, K. Jung, M. Nezafati, C.-S. Kim and B. Kang, *ACS Appl. Mater. Interfaces*, 2016, **8**, 27814–27824.
24 S. Song, H. M. Duong, A. M. Korsunsky, N. Hu and L. Lu, *Sci. Rep.*, 2016, **6**, 32330.
25 P. Colomban, *Solid State Ionics*, 1986, **21**, 97–115.
26 K. Arbi, J. M. Rojo and J. Sanz, *J. Eur. Ceram. Soc.*, 2007, **27**, 4215–4218.
27 A. Martínez-Juárez, C. Pecharromán, J. E. Iglesias and J. M. Rojo, *J. Phys. Chem. B*, 1998, **102**, 372–375.
28 V. S. Kandagal, M. D. Bharadwaj and U. V. Waghmare, *J. Mater. Chem. A*, 2015, **3**, 12992–12999.
29 L. Zhang, K. Yang, J. Mi, L. Lu, L. Zhao, L. Wang, Y. Li and H. Zeng, *Adv. Energy Mater.*, 2015, **5**, 1501294.
30 X.-B. Cheng, R. Zhang, C.-Z. Zhao and Q. Zhang, *Chem. Rev.*, 2017, **117**, 10403–10473.
31 S. Wenzel, T. Leichtweiss, D. A. Weber, J. Sann, W. G. Zeier and J. Janek, *ACS Appl. Mater. Interfaces*, 2016, **8**, 28216–28224.
32 T. E. Ashton, J. V. Laveda, D. A. MacLaren, P. J. Baker, A. Porch, M. O. Jones and S. A. Corr, *J. Mater. Chem. A*, 2014, **2**, 6238–6245.
33 J. V. Laveda, B. Johnston, G. W. Paterson, P. J. Baker, M. G. Tucker, H. Y. Playford, K. M. Jensen, S. J. Billinge and S. A. Corr, *J. Mater. Chem. A*, 2018, **6**, 127–137.
34 M. Månsson and J. Sugiyama, *Phys. Scr.*, 2013, **88**, 068509.
35 A. Keren, *Phys. Rev. B: Condens. Matter Mater. Phys.*, 1994, **50**, 10039–10042.
36 *An Introduction to Solid State Diffusion*, ed. R. J. Borg, G. Dienes, Academic Press, San Diego, 1988.
37 A. Mendiboure, C. Delmas and P. Hagenmuller, *J. Solid State Chem.*, 1985, **57**, 323–331.
38 A. Bhide and K. Hariharan, *Solid State Ionics*, 2011, **192**, 360–363.
39 P. G. Bruce, J. Nowinski and V. C. Gibson, *Solid State Ionics*, 1992, **50**, 41–45.
40 Z. Zhu, I.-H. Chu, Z. Deng and S. P. Ong, *Chem. Mater.*, 2015, **27**, 8318–8325.
41 Z. Yang, J. Zhang, M. C. W. Kintner-Meyer, X. Lu, D. Choi, J. P. Lemmon and J. Liu, *Chem. Rev.*, 2011, **111**, 3577–3613.